J. Meas. Sci. Instrum., 2024, 15(3): 387-396. http://jmsi.publish.founderss.cn/
DOI: 10.62756/jmsi.1674-8042.2024040 jmsi@nuc.edu.cn

Simulation on dynamic characteristics of TC4 cutting with crack defects

SHI Lichen[1], WANG Jian[1*], DOU Weitao[2], YUAN Jiageng[1]

1. School of Mechanical and Electrical Engineering, Xi'an University of Architecture and Technology, Xi'an 710055, China;
2. College of Aeronautical Manufacturing Engineering, Xi'an Aeronautical Polytechnic Institute, Xi'an 710089, China

***Corresponding author:** WANG Jian (15903615309@163.com)

Received: February 2, 2023 **Revised:** April 16, 2023 **Accepted:** April 26, 2023

Abstract: Titanium alloys play an important role in aerospace and other fields. However, after precision forging and cold rolling process, some defects will appear on the subsurface of titanium alloy bars, thus reducing the surface quality and precision of turning process. This study aimed at exploring the effect of crack defects on TC4 cutting. Firstly, the finite element cutting simulation model of TC4 material with crack defects was established in ABAQUS. Then, the cutting parameters such as cutting force, stress concentration, chip morphology, residual stress were obtained by changing the variables such as the size and height of crack defects. Finally, the turning experiment was carried out on centerless lathe. The results show that the cutting force changes abruptly when the defect position is located on the cutting path, the maximal stress occurs at the tip of the defect, and the mutation of stress value is more serious with the increase of defect size; the buckling deformation of chip morphology occurs and becomes less serious with the increase of the distance between the defect position and the workpiece surface; the surface residual stress near the defect is related to the stress when the tool is close to the defect, the larger defect size and the closer to the machined surface, the greater the residual stress. Therefore, under certain processing conditions, the TC4 material should avoid large size defects or increase the distance between defects and the machined surface, so as to obtain better and stable surface quality.

Key words: crack defect; TC4; ABAQUS; centerless lathe

0 Introduction

Since titanium alloy has excellent properties such as light weight, high strength, high temperature resistance, and fatigue resistance[1], it is an important metal material in the fields of aerospace and national defense[2]. Although it has the above-mentioned advantages, the cutting performance of titanium alloy is poor. Therefore, the thermodynamic and dynamic characteristics of titanium and titanium alloy processing have been one of research hotspots[3].

The machinability of titanium alloy has been studied by many scholars, taking into account heat generation and heat conduction in machining. Kong[4] added deformation temperature effect into temperature equation via heat loss, and at the same time, the influence of temperature on deformation was converted into the influence of flow stress on deformation to conduct thermal-mechanical coupling calculation. Wan et al.[5] established different forms of cutting force prediction models such as polynomials and exponential functions by analyzing experimental data. Yang et al.[6] used finite element model to simulate and analyze the whole process of adiabatic shear band formation in titanium alloy TC4 cutting, and obtained serrated chips similar to that by the experiment. He et al.[7] used the energy method to establish a numerical description model of structural parameters, cutting three elements and cutting energy consumption, clarified the formation mechanism of phase transformation on machined surface of titanium alloy, and revealed the regularity of its development. Shen et al.[8] simulated the cutting force and cutting temperature field in turning process, and verified the correctness of the finite element simulation model and the reliability of the simulation results. Tang et al.[9] established a simulation model of multi-step cutting and pre-stressed cutting of titanium alloys, and studied the specific laws of multi-step cutting and pre-stressed cutting process regulation affecting chip shape, cutting force and residual stress of machined surface layer. The results show that both multi-step cutting and prestress cutting can increase the residual compressive stress on the finished surface. The final results of the study showed that when the titanium alloy was cut at a distance of 4.63 mm, the corresponding machine wear was 5.41%. In the application process of porous titanium alloy cutting,

the wear degree caused by titanium alloy cutting is not affected by its cutting distance, and the wear degree caused by titanium alloy cutting has always maintained an average level of about 5.5%, which is relatively stable. However, in practice, due to the characteristics of titanium alloy materials, machining tool marks, defects and tissue damage will appear on the surface of the workpiece during the processing and preparation process[10]. Therefore, the research on defects is a crucial link. Song et al.[11] used finite element method to simulate the bending of two kinds of titanium alloy plates with and without defects respectively, and the results showed that the damage and equivalent strain of the defect plate increased significantly compared with that of the defect-free plate, and hole defects had a great influence on the mechanical properties of the plate. Zhang[12] studied the influence of impurity defects on cutting temperature by finite element method, and the results showed that the microstructure of impurity defects would change the cutting temperature. These results show that the thermodynamic and dynamic characteristics of the materials containing defects will change to a certain extent during the processing, which greatly affects the quality of the machined surface, and then has a negative impact on the processing cycle and cost.

In this study, a finite element model for TC4 cutting was established, and the influence of the variables such as defect size and defect height on cutting force, stress and strain, temperature and surface residual stress in the machining process was analyzed, so as to have a more in-depth understanding of the dynamic cutting process of TC4 material and improve the cutting process.

1 Finite element model

1.1 Geometric model

A two-dimensional orthogonal cutting geometric model is established by ABAQUS finite element software, as shown in Fig.1. The workpiece is composed of cutting area, separation line and matrix. The influence of tool deformation and vibration on numerical simulation results in the actual machining process is ignored. In the cutting simulation model, the rotation and displacement of the workpiece matrix in the X and Y directions are constrained. In addition, the reference point is defined on the cutting tool, and the motion of the tool is applied to the reference point. The cutting tool moves along the reverse direction of the X axis, and the rotation and displacement in the vertical direction are constrained. In addition to the velocity displacement boundary conditions, the cutting tool and workpiece are applied at the initial temperature of 20 ℃.

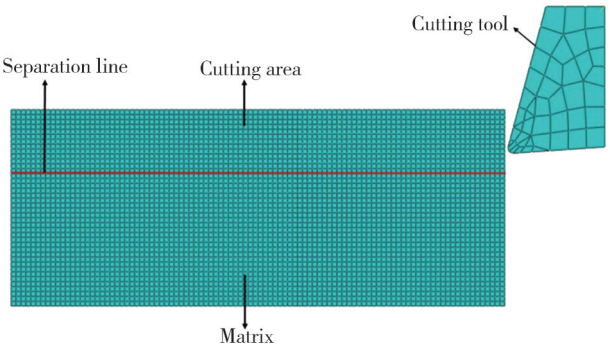

Fig. 1 Two-dimensional finite element model of titanium alloy cutting process

In this study, the cutting tool is defined as rigid body and its deformation is ignored, whereas the workpiece is defined as an elastic-plastic body, and the fine mesh is used in the contact area between the cutting tool and the workpiece to ensure the accuracy of calculation results.

1.2 Johnson-Cook constitutive model

Establishing a reasonable material constitutive model is the key to simulation analysis. There are many constitutive models that describe the thermoplastic deformation behavior of materials at high strain rates, including not only the work hardening effect and temperature softening effect of materials in the processing, but also the strain rate strengthening effect, in which Johnson-Cook model is the most ideal model and can be described by average flow stress as

$$\sigma=(A+B\varepsilon^{n})\left[1+C\ln\left(\frac{\dot{\varepsilon}}{\dot{\varepsilon}_{0}}\right)\right]\left[1-\left(\frac{T-T_{\mathrm{r}}}{T_{\mathrm{m}}-T_{\mathrm{r}}}\right)^{m}\right], \quad (1)$$

where σ is the equivalent stress; ε is the equivalent plastic strain; $\dot{\varepsilon}$ and $\dot{\varepsilon}_{0}$ are the equivalent and reference plastic strain rates, respectively; T, T_{m} and T_{r} are the materials cutting zone temperature, melting temperature and room temperature, respectively; n is the strain hardening index; and m is thermal softening index. Johnson-Cook parameters A, B and C represent the yield strength, strain, and strain rate sensitivity of the material, respectively. The material property were tested and the results are shown in Table 1. Thus material constitutive model is established based on these properties[13].

Table 1 Johnson-Cook constitutive parameters of TC4

Constitutive parameter	Value
Yield strength A/MPa	862
Strain B	331
Strain hardening index n	0.34
Strain rate sensitivity C	0.012
Thermal softening index m	0.8

1.3 Principle of cutting separation

In order to simulate the appearance of chips, the Johnson-Cook failure model is used as a damage initiation criterion. This model takes into account the influence of strain, strain rate and temperature on material failure, and it is expressed as

$$\varepsilon_{\mathrm{f}}^{\mathrm{pla}}=\left[d_1+d_2\mathrm{e}^{d_3\frac{p}{q}}\right]\left[1+d_4\ln\left(\frac{\dot{\varepsilon}}{\dot{\varepsilon}_0}\right)\right]\left[1+d_5\left(\frac{T-T_{\mathrm{r}}}{T_{\mathrm{m}}-T_{\mathrm{r}}}\right)^m\right],\quad(2)$$

where d_1-d_5 are failure parameters that are measured under the transition temperature conditions; $\varepsilon_{\mathrm{f}}^{\mathrm{pla}}$ is the reference strain rate; p is the hydrostatic pressure; and q is the Mises stress.

Table 2 Johnson-Cook failure parameters of TC4

Failure parameter	Value
d_1	0.09
d_2	0.25
d_3	0.5
d_4	0.014
d_5	3.87

2 Finite element cutting simulation with defects

2.1 Finite element model of defects

Defects in materials such as inclusions, holes, and cracks not only affect the integrity of function and performance of the material, but also eventually lead to failure of the material. When these defects appear near the material surface under external load, their damage effect will become more apparent.

In this study, the research object is TC4 formed by rolling, and the defect is crack[14]. The cutting geometric model with crack defects in different regions is established, as shown in Fig.2. The size of the workpiece is 1 mm×0.4 mm, the bottom of the workpiece is completely constrained, the rake angle is 15°, the clearance angle is 4°, the cutting speed is 30 m/min, the width-to-length ratios of the defect size are 1∶5 and 1∶10, respectively. They are located in the shallow zone (above the cutting path).

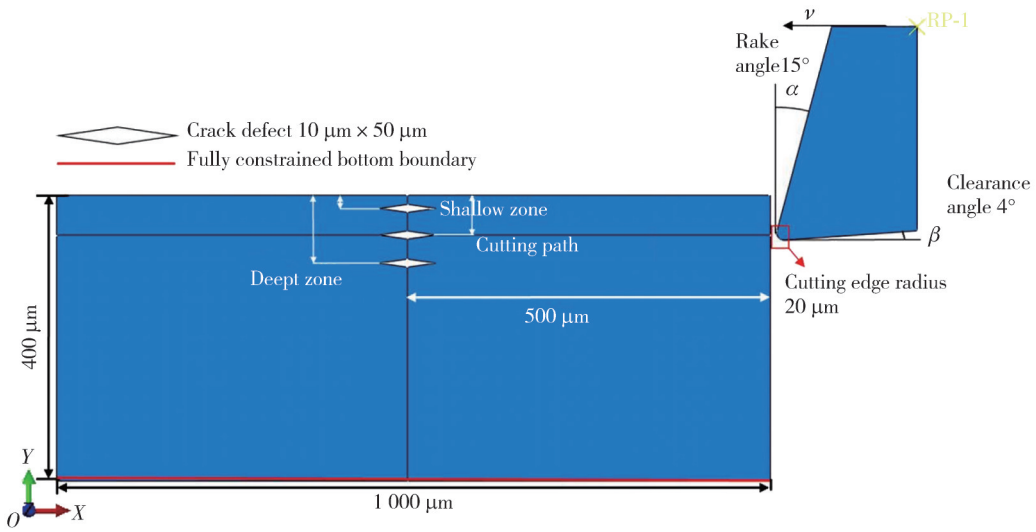

(a) Defects with a ratio of width-to-length of 1∶5

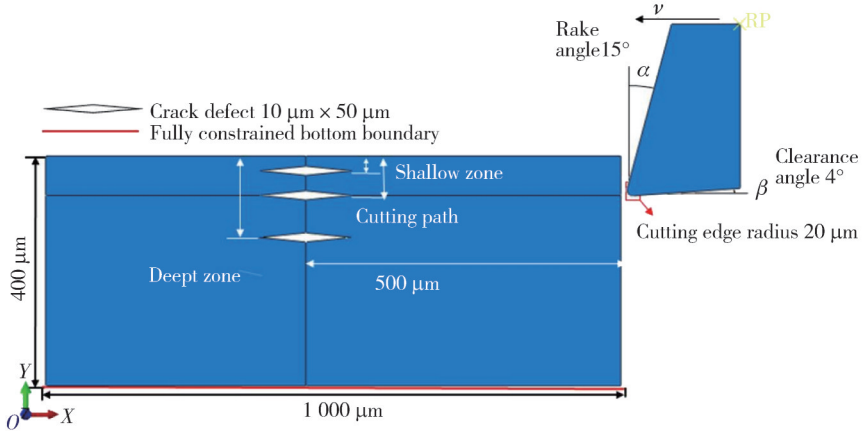

(b) Defects with a ratio of width-to-length of 1∶10

Fig. 2 Cutting geometric model with crack defects in different regions

The cutting path and the deep zone (below the cutting path), respectively.

2.2 Influence of crack defects' position on cutting force

The cutting force changes when crack defects are in different positions: no defect, in deep zone, on cutting path, and in shallow area, as shown in Fig. 3. At the beginning, the cutting tool cuts the workpiece, and the cutting force increases sharply with the increase of the contact area.

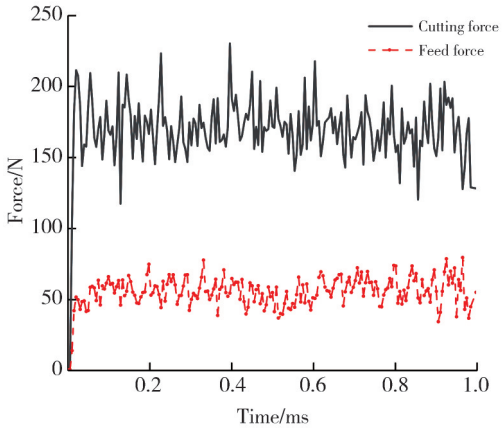

(a) No defect

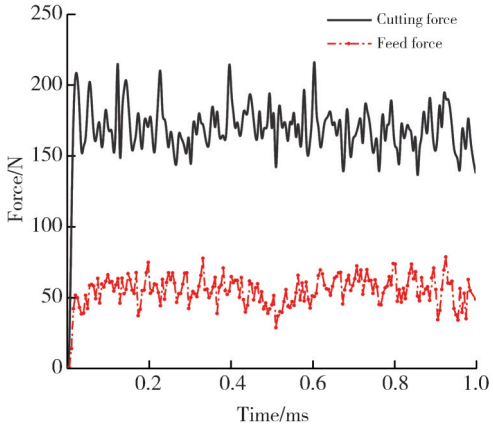

(b) Defects in deep zone

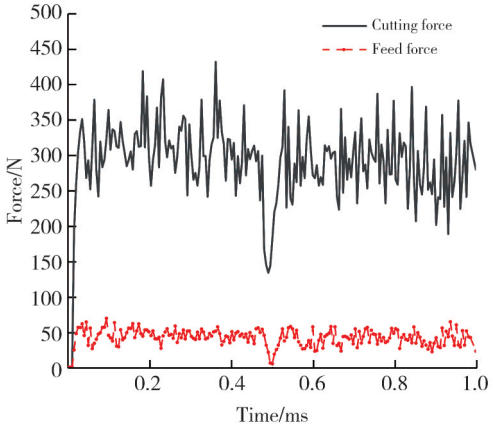

(c) Defects on cutting path

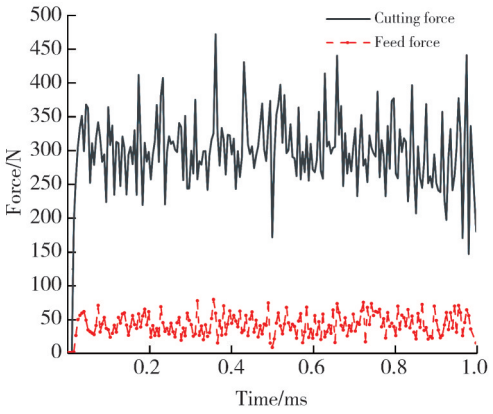

(d) Defects in shallow zone

Fig. 3 Cutting force curves with defects in different conditions

When the yield strength limit of the material is reached, the cutting force drops slightly, and then the cutting reaches a steady state, and the cutting force fluctuates in a cycle. It can be clearly seen from Fig. 3(c) that when the time is close to 0.5 ms, the cutting force has a significant drop mutation, that is, when the cutting tool approaches the cross section of crack defect, the cutting force suddenly drops, which indicates that in a certain cutting depth range, when there are crack defects throught which the cutting tool just cuts, the cutting reaction force of the tool will fluctuate greatly and then affect the mechanical properties of the workpiece. Similarly, the feed force has a similar cutting reaction force fluctuation drop when the time is close to 0.5 ms, and the deeper the defect, the less obvious the mutation.

It can also be clearly found that the black curve has a sudden drop in the same time and has the same trend in Fig. 3(d). The reason is that the internal structure of the material changes with the defects located on the cutting path or in the surface area, resulting in instability of cutting states. On the contrary, the cutting force fluctuations in Fig. 3(a) and (b) display normal trends.

2.3 Influence of crack defects' distribution on stress concentration

In this section, we analyze the influence of the defects' distribution in different conditions on the surface stress, as shown in Fig. 4. We first give a distribution map of defect nodes , including seven equidistant nodes, as shown in Fig. 4(a). From right to left in the horizontal direction, these seven nodes that construct a path, of which node 4 is located at the defect, and other nodes are distributed equidistantly on both sides of the defect in turn, and the stress value of each node on the path is output. In Fig. 4(b) and (c), when the crack defect is located on the cutting path, the stress values of nodes 1—4 increase continuously, the stress value reaches the maximum at node 4 and then it

suddenly drops at nodes 4 — 7. As a result, the stress concentration occurs at node 4, and the stress value has a serious sudden change. When the defect is located in the deep zone and the shallow zone, the stress value at node 4 has a smaller sudden change than that without the defect, and the defects in the shallow zone have a greater influence on the stress value than that in the deep zone. It can be seen from Figs.4 (b) and (c) that with the increase of the width-to-length ratio of the defect, the stress change of the defect on the cutting path becomes sudden and severe. Uneven surface stress distribution has a great influence on surface integrity and surface roughness. Material fatigue cracks are caused by severe stress concentration, which reduces the service life of the material.

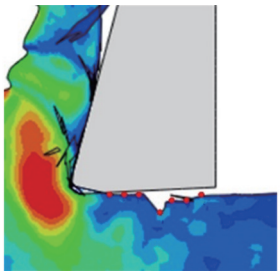

(a) Distribution map of defect nodes

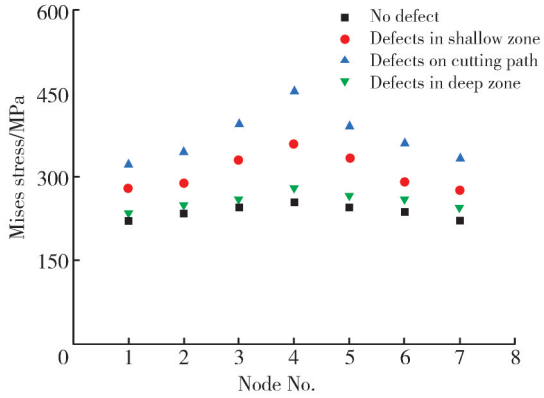

(b) Defects with a width-to-length ratio of 1∶10

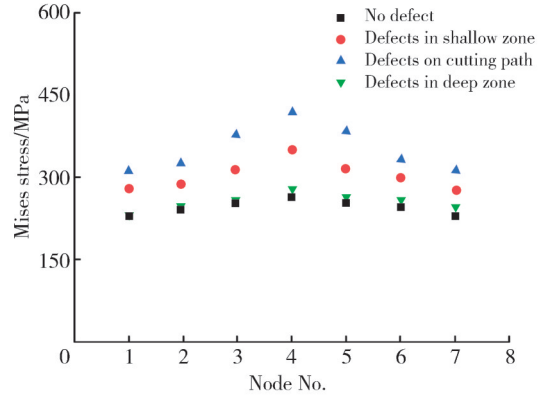

(c) Defects with a ratio of width-to-length of 1∶5

Fig. 4 Mises stress with defects in different positions

Therefore, the internal defects of the material have an impact on the mechanical properties of the workpiece surface after cutting, and the defects located on the cutting path have the greatest impact on the mechanical properties of the surface.

2.4 Influence of crack defects' distribution on chip morphology

Fig.5 shows the chip morphology in different conditions.

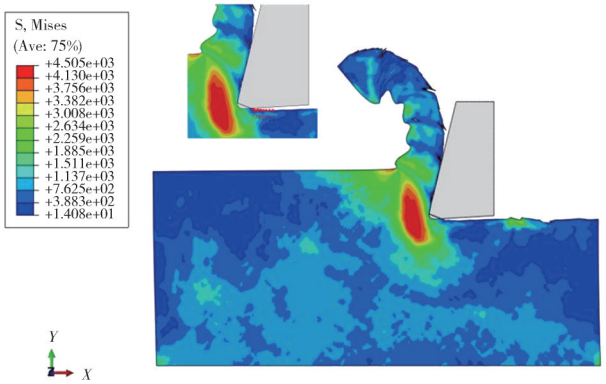

(a) No defects

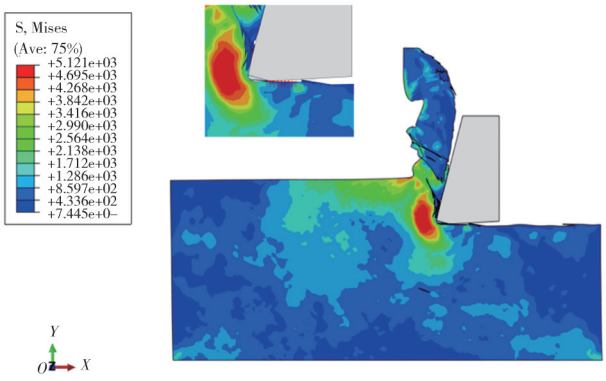

(b) Defects in shallow zone

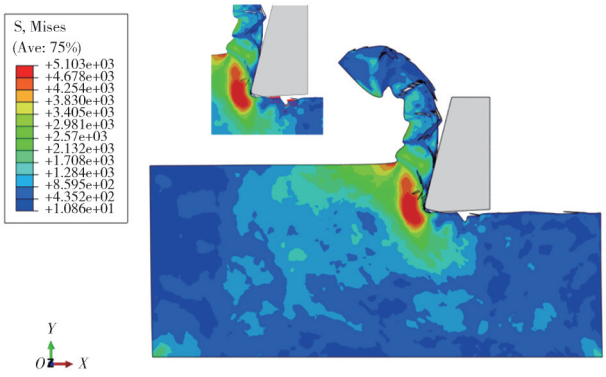

(c) Defects on cutting path

Fig. 5 Chip morphology with defects in different positions

It can be seen that in the absence of defects, the chip is continuously serrated. However, when the defect is located in the shallow zone, the chip morphology is not continuously serrated and the shape is buckled, which may be due to the change in the internal structure of the material caused by the cracks, resulting in local instability of the material. The material not only flows along the shear surface, but also flows to the defect due to the extrusion of the cutting tool, resulting in the change in chip morphology.

When the defect is located on the cutting path, severe chip deformation results in chip fracture. Therefore, the crack defects have an impact on chip morphology in the cutting process, and different conditions have different impacts on chip morphology. Among them, the defects located on the cutting path have the most impact on chip morphology.

2.5 Influence of crack defects' distribution on residual stress

Fig. 6 reveals the influence of the defects on average surface residual stress and residual temperature. It can be seen that the surface residual stress near the defect is related to the stress on the defect surface when the cutting tool is close to the defect, the more the stress loaded on the defect, the more the residual stress retained on the surface.

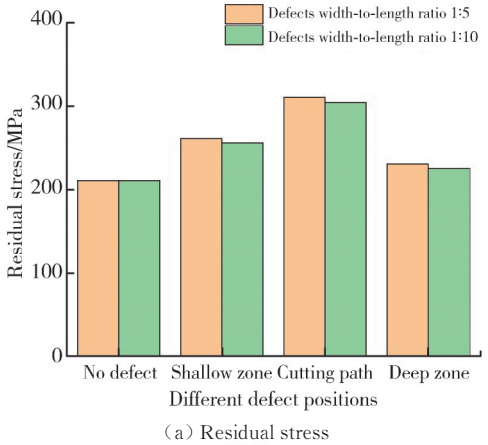

(a) Residual stress

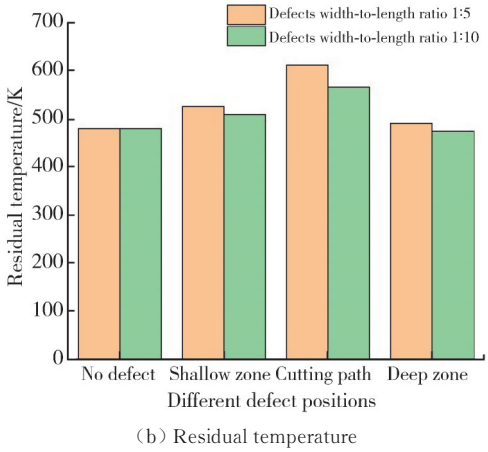

(b) Residual temperature

Fig. 6 Residual temperature and residual stress with defects in different positions

Similarly, the average residual temperature of the defect model on the cutting path is obviously much higher than that of the no-defect model. The average surface residual temperature of the no-defect model is 480 K, the average residual temperature of the model with defects on the cutting path with a width-to-length ratio of 1 : 5 is 566 K, and the average residual temperature of defects on the cutting path with a width-to-length ratio of 1 :10 is 612 K. Therefore, the larger the width-to-length ratio of the defect, the higher the residual temperature. In the cutting simulation, due to the large plastic strain of the metal material in the first deformation zone, a large amount of cutting heat is generated, which is transmitted to the workpiece and the chip by heat conduction. Due to the short contact length between the chip and the cutting tool, the heat is concentrated on the blade and then transferred to the defect.

Fig. 7 shows that the average cutting force of the normal material is 332.4 N, while the average cutting force of the defect with aspect ratio of 1 : 10 is 368.7 N. Therefore, it can be seen that the average cutting force difference is only 36.3 N, and the average residual temperature difference is 132 K, as shown in Fig. 6. It can be simply inferred that the increase of surface residual temperature is not caused by the increase of external cutting force, but may be caused by the existence of defects that change the local stress state of the material in the cutting process. In view of the thermal conductivity of the material and the very short cutting time, it can be known that the heat exchange inside the material is very limited. Therefore, the temperature rise is mainly caused by the existence of defects.

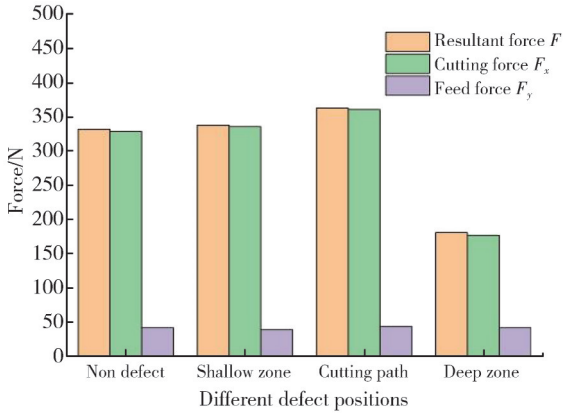

Fig. 7 Force with defects in different positions

3 Experiment

The cutting simulation simplifies various complex conditions and cannot fully consider the complex factors in the cutting process. Therefore, it is necessary to carry out cutting experiments to verify the effect of defects on the cutting process. Shi et al. [15] used the method of measuring the spindle motor current to deduce the variation law of cutting force in titanium alloy cutting process, which solves the problem that the experimental platform of traditional methods is difficult to build. Therefore, the cutting force value can be calculated from

the main motor current in this experiment because not only the main motor current can realize the motor power output, but also the current value is proportional to the cutting force. This experiment considers the situation that the defect is located on the cutting path. The cutting force value derived from the experimental measured current value is compared with the simulation value for verification and analysis.

3.1 Experimental conditions and schemes

The experiment was carried out using XF-WXC lathe and YG8 cemented carbide tools. The specimen selected titanium alloy bar with surface defects and the specimen material was TC4. The real-time monitoring system of lathe was used to record the experimental data, and the data recorded in the turning process included spindle motor current, spindle speed and TC4 bar feed. The experimental setup is shown in Fig.8. The experimental data of the current recorded in the whole cutting process under the same cutting depth and feed rate are shown in Table 3.

(a) Real-time monitoring system (b) XF-WXC lathe

(c) TC4 bar (d) YG8 tool

Fig. 8 Centerless lathe system

Table 3 Cutting conditions used for TC4

Parameter	Value	Description
a_p/mm	0.1	Cutting depth
v/(m•min^{-1})	30	Cutting speed
I/A	33.5—40.7	Cutting current

3.2 Calculation of spindle motor power and cutting force in cutting process

When the spindle speed was 300 r•min^{-1}, the diameter of TC4 bar was 58.3 mm, the cutting depth is 0.1 mm, and the cutting speed was 30 m•min^{-1}, the change of current value can be observed. According to the known power factor and series, K=5.5, as known by Ref.[16], I_0 can be calculated according to the specific parameters of the motor by Eq. (3)[15]. The specific parameters of the spindle motor used are shown in Table 4.

Table 4 Parameters of spindle motor

Parameter	Value	Description
U_N/V	400	Rated voltage
P_N/kW	160	Rated power
I_N/A	268	Rated current
n_N/(r•min^{-1})	1485	Rated speed
n_1/(r•min^{-1})	1500	Synchronous speed
U/V	380	Actual voltage
cos φ_N	0.94	Rated power factor
K	5.5	Series

$$I_0 = K\left[\left(1-\cos\varphi_N\right)\sqrt{1-\cos^2\varphi_N}\right], \tag{3}$$

where I_0 is the no-load current, K is the series, and cosφ_N is the rated power factor.

According to Eqs. (4) and (5)[15], we can get

$$P_1 = \sqrt{\frac{I^2-I_0^2}{I_N^2-I_0^2}}\,P_N, \tag{4}$$

$$P_2 = \sqrt{3}\,UI\cos\varphi\times\eta, \tag{5}$$

where P_1 is the output power of spindle motor, P_2 is the power of spindle motor, I is the output current, I_N is the rated current, U is the actual voltage, cosφ is the power factor, and η is the transmission efficiency of motor.

According to Eqs. (6) — (8)[15], we can get the cutting force value from the measured spindle current, namely

$$P_t = P_2\eta, \tag{6}$$

$$T_t = \frac{9\,550P_t}{n}, \tag{7}$$

$$F = \frac{T_t}{r}, \tag{8}$$

where P_t is the power consumption in tool cutting, n is the spindle speed, T_t is the torque in tool cutting, r is the radius, and F is the cutting force.

3.3 Analysis of experimental results

To effectively verify the reliability of the cutting force obtained in the simulation, the current values of 100 points were measured on the TC4 bar. The maximum measured current value was 39.7 A, the minimum value was 29.5 A, and the average value was 36.9 A, as shown in Fig.9.

It can be seen from Fig.9 that at the initial stage of tool cutting, the current value increases gradually. At the steady-state stage of tool cutting, the current value fluctuates stably at 37.2 A and decreases abruptly at point 50. After this point, the current value is restored to

a stable state, and the change of cutting force is the same trend as that of current value, as shown in Fig.10.

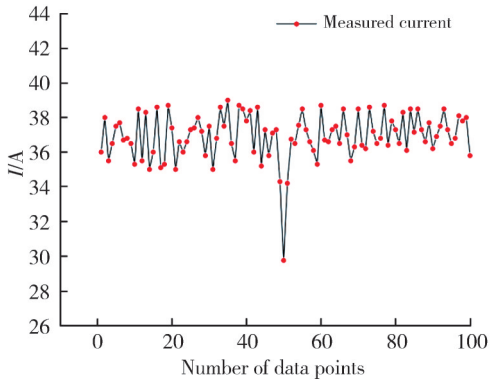

Fig. 9 Measured current by experiment

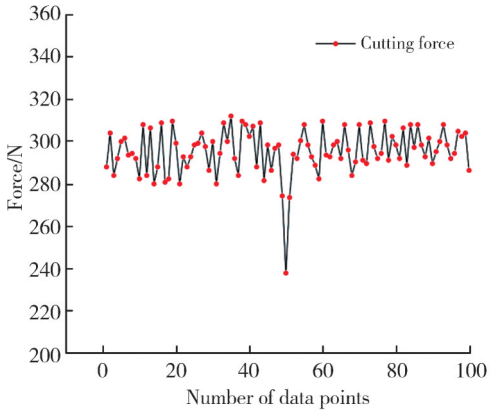

Fig. 10 Measured cutting force by experiment

It can be seen from Fig.10 that the cutting force under experimental conditions has an obvious drop mutation when the defect is on the cutting path. Within a certain range of cutting depth, the defects of the cutting workpiece have an impact on the cutting force, causing the cutting force to fluctuate greatly. The change of cutting force by experiment is the same as that by simulation, which verifies the simulation model well.

3.4 Experimental verification of chip morphology

To verify the influence of defects on chip morphology, a cutting experiment was conducted to observe the chip morphology in different positions of defects, and the experimental results are shown in Fig.11.

It can be seen that when there are no defect in TC4 material, the chip morphology is continuously serrated, as shown in Fig. 11(a). However, when defects are located on the cutting path or in shallow zone, the chip morphology is not continuously serrated and the shape is fractured, as shown in Fig. 11(b) and Fig. 11(c). Hence, the material strength in the cutting area changes, which results in continuous shake of chips and fractures. The simulation result is consistent with the actual chip morphology by the cutting experiment.

(a) Continuous chip morphology (b) Discontinuous chip morphology

(c) Fractured chip morphology

Fig. 11 Chip morphology of defects in different positions

3.5 Experimental verification of residual stress

To verify the results of residual stress simulation, the residual stress measurement was completed under XSTRESS-3000 measuring equipment, as shown in Fig.12.

Fig. 12 X-ray residual stress analyzer

The coordinates of the workpiece were established by taking the initial position of tool tip as the origin of coordinates, the feed direction as the X axis, the row spacing direction as the Y axis, and the normal direction perpendicular to the workpiece surface as the Z axis. Only the residual stress in the X direction was measured. To reduce measurement error, each point was measured three times and the average value was obtained. The parameters and measurements used in cutting experiments are shown in Table 5.

Fig.13 shows the experiment results of residual stress. It can be seen that when the defect's position is on the cutting path, the maximal residual stress appears. With the increase of defect size, the residual stress becomes larger, which is proportional to the defect size. There is a certain gap between the simulation result and the experimental result. The reason is that there are some errors in the measurement result due to the

characteristics of TC4 material during the measurement by X-ray diffraction method. Although there is an error in the numerical value, the simulation result of residual stress is consistent with that in the feed direction, which verifies the simulation model well.

Table 5 Experimental cutting parameters and measurement results

Experiment No.	Defects' position	Width-to-length of defect	Residual stress σ_s/MPa	Average residual stress σ_s/MPa
1			123	
2	No defect		132	123
3			114	
4			143	
5	Shallow zone	1∶5	140	143
6			145	
7			243	
8	Cutting path	1∶5	240	244
9			250	
10			173	
11	Deep zone	1∶5	163	172
12			182	
13			155	
14	Shallow zone	1∶10	149	154
15			158	
16			297	
17	Cutting path	1∶10	290	292
18			288	
19			183	
20	Deep zone	1∶10	178	178
21			174	

spindle speed: 300 r·min^{-1}, cutting speed: 30 r·min^{-1}.

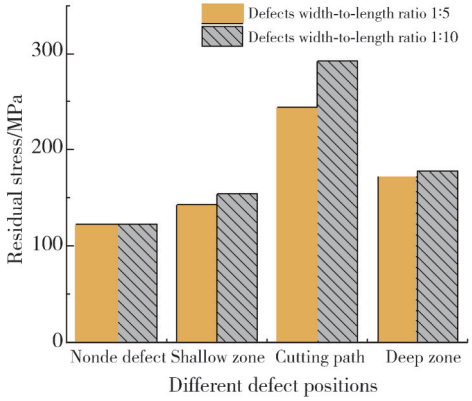

Fig. 13 Experiment results of residual stress

4 Conclusions

In this study, the finite element simulation model of TC4 orthogonal cutting with crack defects was established, and the turning simulation was carried out based on the cutting force characteristics. In addition, the influence of crack defects in different positions of the material on chip morphology, stress concentration and residual temperature in the cutting process was studied, which provides a theoretical basis for the cutting of titanium alloy. The conclusions of this study are as follows:

1) The crack defects inside the material and the defects on the cutting path may cause a mutation in the cutting force, and the maximal stress occurs at the tip of defect. With the increase of defect size, the mutation of the stress was more serious. The simulated cutting force was successfully validated with the experimental result.

2) The difference of defect positions causes the sudden change of surface stress, and the change on the cutting path is more obvious. The maximal stress value occurs at the tip of the defect, and with the increase of defect size, the sudden change in stress becomes more serious.

3) The crack defects in the material change the structure of the material, resulting in the change of chip morphology when cutting to the defect. With the increase of the distance between the defect location and the workpiece surface, the influence on chip morphology becomes smaller.

4) Due to the generation of internal crack defects in the material, the larger the defect size, the more stress retained on the surface when cutting to the crack, and the greater residual stress closer to the defect.

Acknowledgement

This work was supported by Key Research and Development Program of Shaanxi Province (No. 2023-YBGY-386); Natural Science and Technology Fund General Program of Shaanxi Province (No.2021JM-599).

Declaration of conflicting interests

The authors have no conflict of interests related to this publication.

References

[1] HUANG Z K, SUN W. Formation mechanism of adiabatic shear band during dynamic plastic deformation of titanium alloy. Material Report, 2021, 35(3): 3122-3128.

[2] BANERJEE D, WILLIAMS J C. Perspectives on titanium science and technology. Acta Materialia, 2013, 61(3): 844-879.

[3] OUYANG D L, LU S Q, CUI X, et al. Dynamic recrystallization kinetics of deformation in β zone of TB6 titanium alloy. Journal of Materials Research, 2019, 33(12): 918-926.

[4] KONG H X. Numerical simulation and thermodynamic study on high speed orthogonal cutting process of titanium alloy. Taiyuan: North University of China, 2012.

[5] WAN M, ZHANG W H, TAN G, et al. New cutting force modeling approach for flat end mill. Chinese Journal of Aeronautics, 2007, 20(3): 282-288.

[6] YANG Y, KE Y L, DONG H Y. Finite element analysis of

titanium alloy cutting adiabatic shear band formation process. Journal of Zhejiang University, 2008(3): 534-538.
[7] HE G H, WU M Y, LI L X. Research on the formation mechanism and influencing factors of phase transformation of typical titanium alloy cutting layer. Mechanical Engineering Journal, 2018, 54 (17): 133-141.
[8] SHEN X H, ZHANG D H, YAO C F, et al. Research progress on the formation mechanism of surface integrity in titanium alloy cutting. Journal of Aeronautical Materials, 2021, 41(4): 1-16.
[9] TANG R, LING Y. Experimental study on optimization of surface integrity parameters in machining of porous titanium alloys. Internation Journal of Frontiers in Engineering Technology, 2022, 4(7): 68-73.
[10] SUN Q, ZHANG J L, SUN P, et al. Defect Analysis of TC4 Titanium Alloy Forgings. Hot Working Technology. 2018, 47(23): 259-262.
[11] SONG X H, TIAN Y Y, QUAN J K, et al. V-shaped bending of Ti-6Al-4V titanium alloy sheet with elliptical hole. Materials Research Express, 2019, 6(12): 1265j2.
[12] ZHANG X Y. Investigation on of the dynamic deformation mechanism of titanium alloy under the high speed cutting. Taiyuan: Taiyuan University of Technology, 2018.
[13] DUCOBU F, RIVIÈRE-LORPHÈVRE E, FILIPPI E. Application of the coupled Eulerian-Lagrangian (CEL) method to the modeling of orthogonal cutting. European Journal of Mechanics - A, 2016, 59: 58-66.
[14] MIR A, LUO X C, SIDDIQ A. Smooth particle hydrodynamics study of surface defect machining for diamond turning of silicon. The International Journal of Advanced Manufacturing Technology, 2017, 88(9): 2461-2476.
[15] SHI L C, DU X Y, DOU W T, et al. Experimental research on the empirical formula of titanium alloy cutting force based on the current of the spindle motor of a centerless lathe. Machine Design and Manufacturing, 2017 (3):261-263.
[16] YANG B W, ZHOU Z G. Measurement and correct application of motor load rate. Development and Innovation of Mechanical and Electrical Products, 2003(6): 24-25.

裂纹缺陷下TC4切削加工动态特性仿真

史丽晨[1], 王 简[1*], 豆卫涛[2], 袁嘉庚[1]

1. 西安建筑科技大学 机电工程学院, 陕西 西安, 710055;
2. 西安航空职业技术学院 航空制造工程学院, 陕西 西安, 710089

摘 要: 钛合金在航空航天等领域发挥着重要作用。由于精锻、冷轧后的钛合金棒材亚表面易产生裂纹缺陷,本研究将探究其对TC4材料切削加工的影响。首先,利用ABAQUS构建了含裂纹缺陷的TC4材料有限元切削仿真模型。其次,通过改变裂纹缺陷的尺寸和高度等变量得到切削力、应力集中、切屑形状、表面残余温度和残余应力等参数。最后,在无心车床上进行了切削实验。结果表明,当裂纹缺陷位置处于切削路径时,切削力会产生突变,在缺陷尖端点处出现最大应力值,且应力值随裂纹尺寸增大而增大;切屑形态也发生了屈曲变形,其随缺陷位置与工件表面距离的增加而减小;裂纹缺陷附近的表面残余应力与裂纹尺寸大小和刀具靠近缺陷时的应力大小相关,尺寸较大且靠近加工表面的缺陷会导致更大的残余应力。因此,在加工条件一定的情况下,钛合金材料应避免出现尺寸较大的缺陷或者通过增加缺陷与加工表面之间的距离,以确保良好和稳定的表面质量。

关键词: 裂纹缺陷; TC4; ABAQUS; 无心车床

引用格式: SHI Lichen, WANG Jian, DOU Weitao, et al. Simulation on dynamic characteristics of TC4 cutting with crack defects. Journal of Measurement Science and Instrumentation, 2024, 15(3): 387-396.